Journal of Stress Analysis
Vol. 2, No. 2, Autumn – Winter 2017-18
Bu-Ali Sina University

Influence of Hardening on the Cyclic Plastic Zone Around Crack Tip in Pure Copper CT Specimens

R. Hosseini, R. Seifi*
Mechanical Engineering Department, Bu-Ali Sina University, Hamedan, Iran.

Article info

Article history:
Received 03 January 2018
Received in revised form
10 March 2018
Accepted 12 March 2018

Keywords:
Nonlinear hardening
Cyclic plastic zone
Crack tip
CT specimen

Abstract

Under cyclic loading, the plastic zone becomes complicated during unloading. The energy-absorbing cyclic plastic zone is a stimulant for crack growth and can be a criterion for determining the damage around the fatigue crack tip. Presenting analytical models for determining the shape and size of the plastic zone often makes restrictive assumptions such as elastic-perfectly plastic response. In this research, the effects of non-linear kinematic hardening behavior of pure copper on the cyclic plastic reaction of the crack tip in different conditions were investigated. Chaboche nonlinear material model was used to determine the hardening parameters. According to the numerical results, the cyclic plastic zone around the crack tip was constant in the same load range but load ratio had a slight effect on this zone. Moreover, presence of the kinematic hardening in the cyclic loading caused reverse plastic zone to be predicted smaller than analytical model. According to the results, for materials such as pure copper with kinematic hardening behavior, the cyclic plastic zone increases with increase in the crack length. Therefore, the cyclic plastic zone, as well as other parameters in the fracture mechanics can be a proper criterion for fatigue crack growth studies.

Nomenclature

X	Total back stress	v	Poisson's ratio
X_i	Decomposed back stress	CT	Compact tension
C	Kinematic hardening coefficient	B	Thickness
γ	Kinematic hardening exponent	W	Width
dP	Equivalent plastic strain increment	K_{max}	Maximum stress intensity factor
$d\varepsilon^p$	Plastic strain increment	K_{min}	Minimum stress intensity factor
ε_x^p	Plastic strain	ΔK	Stress intensity factor range
σ_x	Stress in cyclic stress-strain diagram	c_{pc}	Cyclic plastic zone size
σ_0	Cyclic yield stress	a	Crack length
ε_L^p	Plastic strain limit	ΔP	Load range
$r_p(\theta)$	Plastic zone size in θ direction	R ratio	Ratio of minimum and maximum load
s_Y	Yield stress		

*Corresponding author: R. Seifi (Associate Professor)
E-mail address: rseifi@basu.ac.ir
http://dx.doi.org/10.22084/jrstan.2018.15449.1037
ISSN: 2588-2597

1. Introduction

In fracture mechanics, most of the studies are based on the description of growth of the cracks. In materials which the plastic zone is small in comparison with specimen dimensions, the assumption of linear elastic fracture mechanics, known as LEFM, is valid. In such cases, the concept of the elastic stress intensity factor range ΔK, which is fatigue crack growth driving, is used [1]. In many loading conditions, linear fracture mechanics is incapable of describing the stress fields of the crack tip. In these cases, there are limited elastic-plastic analyses that evaluate large-scale yielding around the crack tip. Understanding the plastic zone around the crack tip is of great importance in the fatigue loading. The large plastic zone absorbs a large amount of energy during crack propagation and its small size means that the crack propagation requires less energy. The plastic zone plays an important role in the material damage. The studies which investigate the rate of the fatigue cracks are generally based on the mechanical parameters such as ΔK or displacement at the crack tip, CTOD. During fatigue cracking, two plastic zones around the crack tip are created. One is a monotonic plastic zone during loading and the other is the cyclic plastic zone (CPZ) during unloading-reloading stages. The size and shape of the plastic zone produce effect on the behavior of the crack growth.

Under cyclic loadings, there are three different zones around the crack tip as depicted schematically in Fig. 1. In first region, hysteresis loop is complete and shape of the loop depends upon R-ratio (here, the ratio of minimum to maximum stress intensity factors) and ΔK. Second region located exactly after this CPZ, which is known as monotonic plastic region. In this part, the plastic deformation and unloading occur during initial monotonic loading and thereafter the elastic loading. The third zone is positioned far ahead of the crack-tip and material has elastic behavior [2].

Mishra and Parida [3] used elastic-plastic finite element analysis on a thin center cracked plate for determining the plastic zones near the crack tip. The shape and size of the plastic zones at the crack tip for four stress levels were obtained. It was observed that plastic zone sizes based on Tresca yield criterion is relatively bigger in comparison with Von-Mises criterion. The results showed that the tilt angle of the largest plastic-zone radius with respect to the crack axis decreases slightly with increasing the applied stress level. Lino [4] showed that in steels, there is a relationship between the fatigue crack growth rate and plastic zone. In this model of the crack growth, the effect of the plastic zone, which residual stresses affected on it, was investigated. It was shown that with propagation of the crack, the plastic zone is enlarged. McClung [5] with elastic-plastic finite element simulation studied the size of the monotonic and reversed plastic zones at the crack tip. He showed that the width of the monotonic plastic zone at the fatigue crack tip is not influenced by closure. But the width of the reversed plastic zone in the plane stress condition, due to the fatigue crack closure, is less than one-fourth of the size of the monotonic plastic zone. Linear hardening behavior was also considered based on the monotonic results of tensile test.

Irwin [6] and Dugdale [7] provided analytical models for estimating the crack tip plastic zone size in an infinite plate with central crack. In the presented models, the material behavior was assumed as elastic-perfectly plastic. Jingjie et al. [8] estimated cyclic plastic zone size by maximum crack opening displacement, MCOD and its variable value, VMCOD. They used 2D elasticplastic finite element analysis to quantify the cyclic plastic zone size for a center-cracked plate subjected to cyclic tensile loads. A simple function relationship of the cyclic plastic zone size was utilized versus MCOD for elastic-perfectly plastic materials, which were independent of the plate width, crack length, elastic modulus, yield stress, and stress ratio under constant amplitude loads.

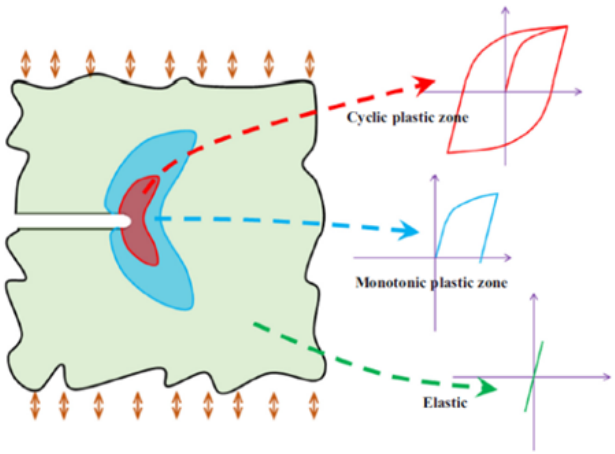

Fig. 1. Induced zones and their responses around the fatigue crack-tip [2].

Chikh et al. [9] studied the CPZ size and fatigue crack growth rate, FCGR on 12NC6 steel. The results of their research showed that, generally, with crack growth, the plastic zone size increased and FCGR was correlated with the energy absorbed in these plastic zones.

Kwun and Fine [10] used the strain-gauge method to measure the plastic zone size of powder metallurgy aluminum alloy MA87 under cyclic loading at various. In the foil strain-gauge technique, a tiny strain-gauge is situated on the specimen so that it is parallel to the loading direction ahead of the crack-tip. During loading, the output of the strain-gauge is recorded as a stress-strain diagram. When strain becomes nonlinear, the distance from the crack-tip until the strain-gauge center is determined as the plastic zone size. In ex-

perimental techniques for determining plastic zones, it is very difficult to separate the CPZ from the monotonic. Moreover, many of the numerical models, which are used to determine the cyclic plastic behavior of materials, use isotropic hardening rule as the material elastic-plastic response [3,11-13]. Isotropic hardening rule cannot predict some of the cyclic behavior of the materials, such as the effects of Bauschinger effect, ratcheting and release of mean stress, which occur in real materials [14-16]. Therefore, for accurate determination of the cyclic and monotonic plastic zones, usage of the finite element methods is very beneficial.

In many analytical and numerical models, material behavior is considered elastic-perfectly plastic. In some numerical models which consider elastic-plastic behavior, the hardening behavior is calculated based to the monotonic stress-strain curve. But in this research, the hardening behavior of the material based on the cyclic stress-strain curve was determined according to the Chaboche model [17]. Furthermore in this research, cyclic plastic zone was determined based on the back stresses variations in the cyclic loadings. To evaluate the advantages of this method, the cyclic plastic zone obtained from finite element analysis was compared with the predicted values by Irwin analytical model.

2. Nonlinear Kinematic Hardening Model

If the stress exceeds the elastic limit and the loading continues, the hardening of the material may occur in two forms: the kinematic hardening, which the yielding surface is transferred in the deviation stress space and the isotropic hardening at which the yielding surface is expanded. In fact, a complete plastic model consists of the following three main parts: 1. The yield function, which is a mathematical relation, based on the stress components that lead to the formation of the plastic flow in the material. 2. The flow rule, which expresses the relationship between the stresses and plastic strains. 3. Hardening rule that expresses how to change the yield function with the plastic strains and its amount.

Hitherto, numerous numerical models have been proposed to predict the plastic behavior of the materials [17-21]. The Chaboche nonlinear kinematic hardening model, which is used to examine the cyclic plastic behavior of the materials, can predict cyclic properties such as Bauschinger effect, cyclic hardening or softening, ratcheting, and releasing of mean stress. The Chaboche kinematic hardening model is superposition of several back stress terms in the form of the Armstrong-Frederick relationship [18], which each expression simulates one part of a cyclic stress-strain curve. The Armstrong-Frederick model and the Chaboche plastic pattern are written in the form of the equations 3 and 4, respectively.

$$dX = (2/3)Cd\varepsilon^P - \Gamma X dP \tag{1}$$

$$dX = \sum_{i=1}^{m} dX_i, \qquad dX_i = \frac{2}{3}C_i d\varepsilon^P - \gamma_i X_i dP \tag{2}$$

where X is back stress, C_i and γ_i are the material parameters that are obtained from the experiment. The equivalent plastic strain increment, dP, is obtained from equation 3.

$$dP = \left(\frac{2}{3}d\varepsilon^P : d\varepsilon^P\right)^{1/2} \tag{3}$$

Bari and Hassan [21] used hysteresis loop of the cyclic loading to identify the parameters of Chaboche model. The equations for determining the stress at each point are presented in equations 4 and 5.

$$\sigma_x = \sigma_0 + \sum_{i=1}^{3} X_i \tag{4}$$

$$X_3 = C_3\varepsilon_x^P, \tag{5}$$

$$X_i = (C_i/\gamma_i)\left[1 - 2\exp\left\{-\gamma_i\left(\varepsilon_x^P - (-\varepsilon_L^P)\right)\right\}\right] \quad i = 1, 2$$

By summing of the three rules in equation 4 and 5, the stress is determined according to equation 6.

$$\sigma_x = \sigma_0 + \left(\frac{C_1}{\gamma_1}\right)\left[1 - 2\exp\left\{-\gamma_i\left(\varepsilon_x^P - (-\varepsilon_L^P)\right)\right\}\right] \tag{6}$$

$$+ \left(\frac{C_2}{\gamma_2}\right)\left[1 - 2\exp\left\{-\gamma_i\left(\varepsilon_x^P - (-\varepsilon_L^P)\right)\right\}\right] + C_3(\varepsilon_x^P)$$

where ε_L^P is the plastic strain limit of the stable hysteresis loop, σ_0 is the cyclic yield stress and ε_x^P is the plastic strain at each point of the cyclic stress-strain diagram.

3. Experiments

In this paper, cyclic and tensile test specimens were prepared from copper sheet with 5mm thickness. Measured ingredients of this material are presented in Table 1. The reason for choosing copper is its application in industry, high ductility, and its hardening behavior. This metal is the base element of many alloys and studying its responses under cyclic loadings is important.

Table 1
Yield stress, ultimate stress, and elongation for overlapping FSP samples.

Zn	Pb	P	Mn	Fe	Ni	Si
< 0.01	< 0.01	< 0.003	0.01	0.01	0.01	0.01
Cr	Al	S	Co	Cu		
Trace	0.002	None	0.02	> 99.9		

Cyclic test specimens were prepared according to the standards ASTM E606 [22] and Wire cut process was used in making specimens. In this method, due to electrical current in the wire of titanium with 0.1mm diameter, not any contact is established between cutter and specimen. As a result, no significant residual stress will be created due to machining. After machining operation, all of specimens were polished by water proof polishers with different roughness degrees.

For studying the cyclic plastic behavior, standard dumbbell-shaped specimens were subjected to cyclic loading as depicted in Fig. 2. Experiments were performed using Zwick/Roell servo-hydraulic test machine. The specimens were carefully tightened to machines fixtures and adjusted. Tests were done under 0.005Hz frequency. The reason to choose low frequency is providing more data for analysis (200 seconds for each cycle). First, according to specimen dimensions and mechanical properties, several specimens were subjected to loading with various amplitudes to adjust the machine. Finally, according to initial tests, strain range of 1.1% was selected for symmetric strain-controlled cyclic tests. According to the settings, at least 400 points per cycle were obtained for analysis.

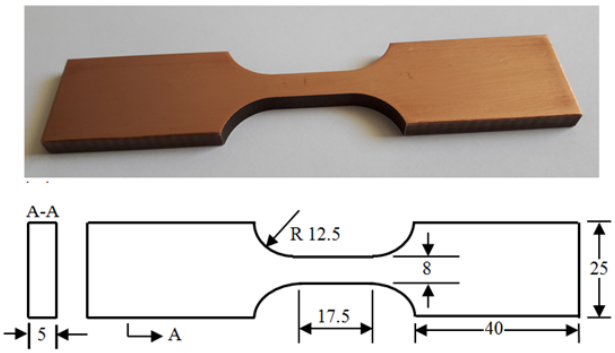

Fig. 2. A cyclic test specimen and its geometry (dimensions are in mm).

Based on the experiments, hysteresis loops in symmetric strain-controlled loading were found for specimens. Experiments were continued until stabilization of hysteresis loops. Obtained hysteresis loops are shown in Fig. 3.

For using the relations (4-6), the stable hysteresis loop is used for determining the parameters of the nonlinear kinematic hardening model. The stable hysteresis loop is separated, and the analysis is performed on the loading branch of this loop. From the starting point of loading, a parallel line with the linear part of the diagram is drawn; the first point on the curve that is deviated from the line is considered as the yield stress. The plastic part of the loop begins from this point and continues to the endpoint of the loading branch. The three hardening rules are applied to the plastic range. C_1 is large enough to model a large slope at the beginning of the yield region, and γ_1 is also sufficiently large to stabilize the first rule and can simulate the knee part of the loop. The third rule is linear and with assumption of $\gamma_3 = 0$ passes from the origin, thus its slope C_3 is equal to the slope of linear end part of loading branch. C_2 and γ_2 must be in such a way as to satisfy the model parameters of equation 7.

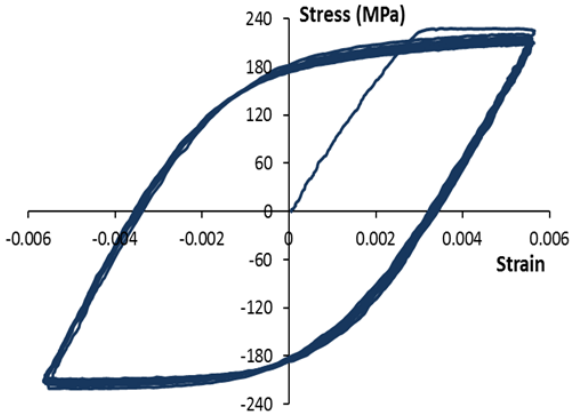

Fig. 3. Hysteresis loops (engineering stress-strain) in condition of symmetric strain controlled test for pure copper material.

$$\frac{C_1}{\gamma_1} + \frac{C_2}{\gamma_2} + \sigma_0 = \sigma_x - (C_3/2)\{\varepsilon_x^p - (-\varepsilon_L^P)\} \qquad (7)$$

In equation (7), ε_x^p is the plastic strain at the points around the end of the plastic zone. The sum of these rules (total back stresses) with initial yield stress (the beginning of the plastic region) simulates the overall stress of the hysteresis loop. After calculating parameters of these three rules, the relationship between the stress σ_x and the plastic strain ε_x^p in the hysteresis loop is determined according to the equation (6). In Figure 4, experimental and simulated stable hysteresis loops based on a nonlinear kinematic hardening model are presented. The comparison of results shows that the simulated model has sufficient accuracy.

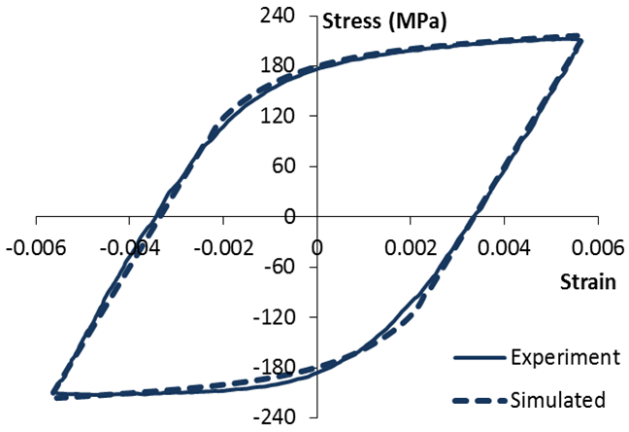

Fig. 4. Experimental and simulated stable hysteresis loop of pure copper.

In this study, the kinematic hardening behavior of

the material for the stabilized hysteresis loop (as depicted in Fig. 4) is determined. The calculations are based on the relationships in section 2 and the method that presented in section 3. The calculated parameters based on Chaboche nonlinear kinematic hardening model are presented in Table 2.

Table 2
Parameters of Chaboche nonlinear kinematic hardening model.

Cosntant	Value
σ_0(MPa)	91
C_1(MPa)	71470
C_2(MPa)	59653
C_3(MPa)	3150
γ_1	8920
γ_2	667
γ_3	0

4. Analytical Models for the Plastic Zones Around the Crack Tip

The shape of the plastic zone is obtained by calculating the radius of plastic area with considering the proper yield criterion versus different value of position angles, θ. In this method, the approximate shape of the plastic zone is estimated by finding the locus of the points for which the elastic stresses fields satisfy the yield criterion. By using the singular stress field (which is based on the stress intensity factor and distance from the crack tip) and Von-Mises yield criterion, the expansion of the plastic zone as a function of θ is obtained by using the equations 8 and 9, for the plane strain and plane stress conditions, respectively [23].

$$r_p(\theta) = \frac{K_I^2}{4\pi S_Y^2}\left[\frac{3}{2}\sin^2\theta + (1-2v)^2(1+\cos\theta)\right] \quad (8)$$

$$r_p(\theta) = \frac{K_I^2}{4\pi S_Y^2}\left[1 + \frac{3}{2}\sin^2\theta + \cos\theta\right] \quad (9)$$

This method is based on a simple yield criterion and does not consider any stress redistribution due to the plastic deformations. Therefore, it is an approximate method. Irwin model is a correction method for the size of the plastic zone and estimates the plastic zone ahead of the crack tip for the cases of plane stress and plane strain under small-scale yielding. According to Irwin's theory [6], corrected length of the plastic zone in front of the crack tip for the plane stress and plane strain conditions are presented in equations 10 and 11, respectively.

$$c = \frac{1}{\pi}\left(\frac{K_I}{S_Y}\right)^2 \quad (10)$$

$$c = \frac{1}{3\pi}\left(\frac{K_I}{S_Y}\right)^2 \quad (11)$$

In these equations, c is the size of the plastic zone and K_I is the mode I stress intensity factor, which is defined in equation 12 for the CT specimen [24].

$$K_I = \frac{P}{B\sqrt{W}}\frac{(2+\alpha)}{(1-\alpha)^{3/2}}(0.886 + 4.64\alpha - 13.32\alpha^2 + 14.72\alpha^3 - 5.6\alpha^4) \quad (12)$$

where P is the applied load, B is the thickness, W is the CT specimen width, $\alpha = a/W$ and a is the crack length.

In the model presented by Dugdale, the plastic zone is corrected for materials with elastic-perfectly plastic behavior that follows Tresca criterion. The Dugdale model [7] is based on the strip model offered for very thin plates (plane stress condition). The length of the plastic zone is obtained by equation (13).

$$c = \frac{\pi}{8}\left(\frac{K_I}{S_Y}\right)^2 \quad (13)$$

In cyclic loading, the stress intensity factor varies from K_{max} during the loading stage to K_{min} at the end of the unloading stage, therefore stress intensity factor changes according to $\Delta K = K_{max} - K_{min}$. Considering elastic-perfectly plastic behavior, the stress range varies by twice of the monotonic yield stress (range from $+S_Y$ to $-S_Y$). For plane strain condition, according to the Irwin model, the size of the CPZ is determined by equation 14.

$$c_{pc} = \frac{1}{3\pi}\left(\frac{\Delta K}{2S_Y}\right)^2 \quad (14)$$

5. Numerical Modeling of the Plastic Zones

It is quite difficult to experimentally determine the cyclic plastic zone around the crack tip. Moreover, analytical relations give approximate values only ahead of the crack tip. In the Irwin and Dugdale models, the plastic zone in front of the crack tip is measured along with the crack line and the shape of this zone assumed circular, regardless of the actual shape of the zone. In these models, there is no singular stress and elastic-perfectly plastic behavior is assumed for materials. The actual size and shape of the plastic zone that are due to the elastic-plastic behavior in monotonic loading can be achieved through the numerical solutions.

5.1. Finite Element Model of CT Specimen

Two-dimensional finite element models were constructed for simulating of compact tension (CT) specimens (width = 25mm, height = 24mm and thickness = 5mm) with various crack lengths. Seven models with

crack lengths of 7, 7.5, 8, 8.5, 9, 9.5, and 10mm were constructed. These models with various crack lengths were designed for evaluating of the cyclic plastic zones which were affected by the crack length. Commercial finite element package, Abaqus, was used in this study. The material model parameters described in sections 3 and presented in Table 2 were introduced to the finite element software. Eight-node nonlinear elements under plane strain condition, CPE8R, with reduced integral technique were used in meshing of the model. The elements were quad shape created by the sweep and free techniques. Fig. 5a shows overall meshing of the CT specimen. In the near-tip regions, the refined meshes were used to capture the large strain gradients due to presence of the crack. The elements sizes in the zone around the crack tip were sufficiently small and decreased linearly with the elements approaching the crack tip, as shown in Fig. 5b. In the present study, the smallest element size reaches 0.5μm at the crack tip to achieve the convergence of the solutions. The model had 7104 elements inside a circle with a radius of 1 mm in the center of the crack tip. For every model, the maximum loads were imported in the load module in the software and then tabular data was imported for define of the load ratio. In step module, every cycle was specified with 50 evenly spaced time intervals. The high number of intervals allows analyzing the results with more detail.

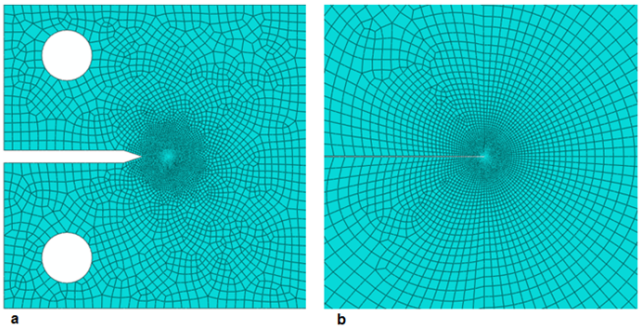

Fig. 5. Finite element model mesh a) CT specimen, b) Meshes around the crack tip.

5.2. Plastic Zones

In CT specimens with different crack lengths, the plane strain analysis was performed. In each crack length, by fixing of the maximum load Pmax and change in the loading ratio R, the plastic zone was determined. Furthermore, proper analyses were performed on the model by fixing the loading range, P, and changing the load ratio. The region around the crack tip, which is being plastic in the tensile loading of the first cycle, is considered as a monotonic plastic zone (MPZ). At the maximum load, it is assumed that the common boundary between the plastic and elastic zones are created in the equivalent plastic strain equal to 5×10^{-6}. A region around the crack tip in which the plastic strain is greater than 5×10^{-6} is defined as the MPZ. This zone is also accessible at places around the crack tip, which have non-zero back stress in the loading direction, a_{22}, and has the same results as monotonic loading. In Fig. 6, for example, the MPZ around a crack with $a = 8$mm under maximum load, $P_{max} = 1200$N, is depicted based on the equivalent plastic strain and back stress. As can be seen, there is no considerable difference between the results for the size of the monotonic plastic zone.

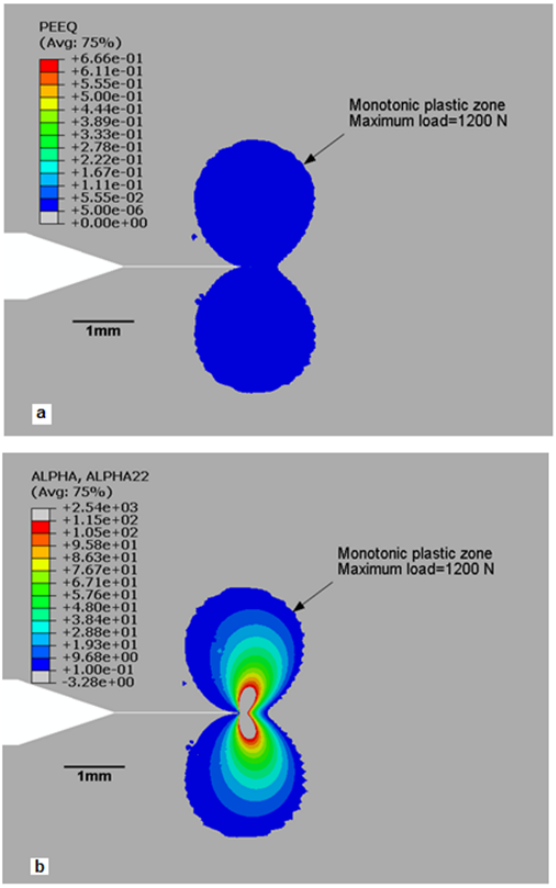

Fig. 6. Monotonic tensile plastic zone at maximum load, a) With equivalent plastic strain (PEEQ), b) With back stress on loading direction (a_{22}).

The test material has a kinematic hardening behavior and due to the plastic behavior of the material in cyclic loading, back stresses are generated around the crack tip. In cyclic loadings in far regions from cracks, the behavior of the material is elastic, but when we approach the crack tip, the behavior of the materials becomes plastic, and in the region that contains closed stress-strain loop (hysteresis loop), the CPZ is created. In fact, in the region where loading leads to hysteresis loops, the back stresses change over the cycles. Therefore, the CPZ can be drawn on the basis of a criterion that back-stress in the loading direction changes between maximum and minimum peak stresses [16]. In Fig. 7, the back stress contours are shown for maxi-

mum and minimum loads on CT specimen with crack $a = 8$mm and loading conditions as $P_{max} = 1200$N and $R = 0.1$. As can be seen, there are considerable variations in the stresses near the crack tip due to the change of the loading from maximum to minimum values. However, in far regions, back stress distribution does not show variations. In Fig. 7b, the white border line shows the shape of the CPZ approximately. Fig. 8 shows the back stress variations due to applying the minimum and maximum loads versus distances from crack tip. It can be seen that the curves for maximum and minimum loads for each condition coincide after some distances from crack tip, which means after that the back stresses do not change over the cyclic loading. The distance from the crack tip to this point of intersection in desired direction is assumed as the CPZ.

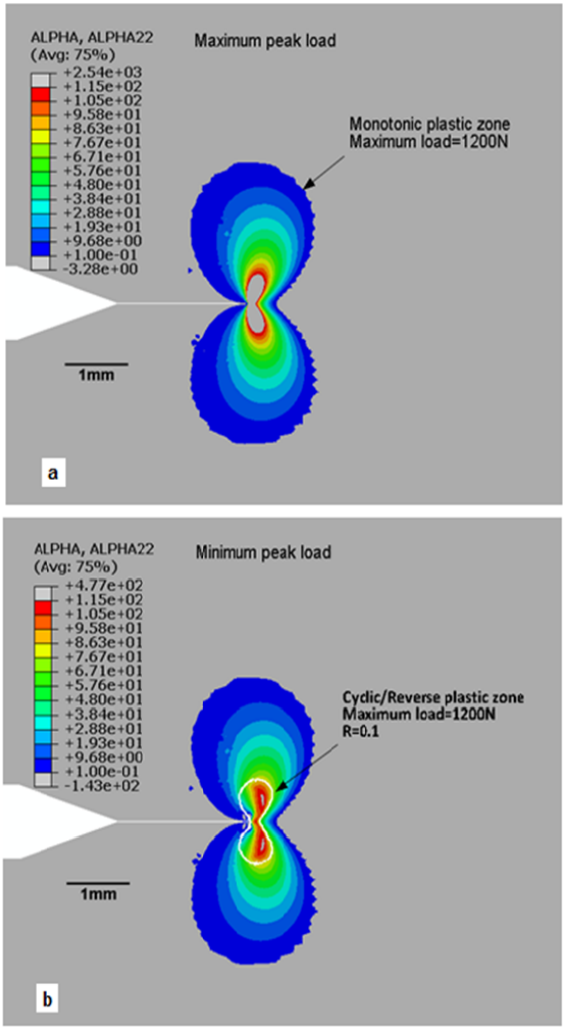

Fig. 7. Back stress contours in pure copper CT specimen with a crack, a) At maximum load of $P_{max} = 1200$N, b) At minimum load with load ratio, $R = 0.1$.

For a more precise study of the shape of the CPZ, in several directions, back stress variations were investigated. By specifying the intersection of simulated diagrams, the shape of the CPZ is characterized by the presented method. In Figs. 9-11, the CPZ is presented in various loading conditions. In fact, the plastic zone is symmetrical relative to the crack surface, so only the upper part of the CPZ is shown here. The investigations were conducted in several crack lengths, but in Figs. 9-11, the results are shown for four crack lengths. In Fig. 9, the maximum load is and the load ratio is 0.1 and 0.3 while in Fig. 10 we have $P_{max} = 1200$N. In Fig. 11, the load range is $\Delta P = 1200$N with the load ratios as 0.077 and 0.2.

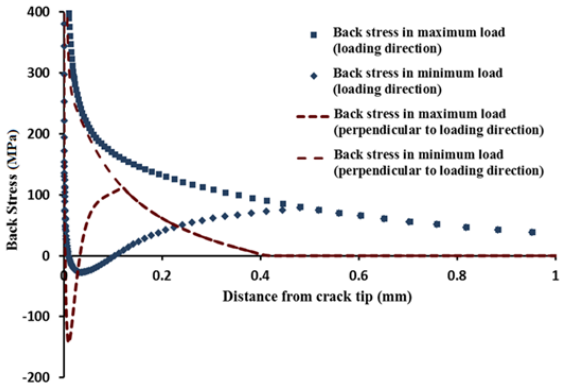

Fig. 8. Variation of back stresses versus distance from the crack tip at minimum and maximum loads.

To compare the CPZ in different conditions, the width and height of the CPZs were determined from obtained contours in Figs. 9-11. These results for conditions of $P_{max} = 1.2$kN, $P_{max} = 1.5$kN and $\Delta P = 1.2$kN with different load ratios are shown in Figs. 12a, 12b and 13, respectively.

With respect to Fig. 12, the CPZ size (CPZS) increases by constant maximum load of P_{max} and decrease in the load ratio. This indicates that the CPZS is correlated with the load range. In Fig. 13, the CPZS (width and height) is presented under the same load condition, $\Delta P = 1.2$kN and different load ratios, $R = 0.077$ and $R = 0.2$, are equivalent to the loading conditions of Fig. 11. According to the results of the numerical models, in all investigated cases, CPZS increases when the length of the crack increases. With respect to Fig. 13, the values of CPZS in each crack length are approximately equal with the same load ranges. This is consonant with analytical results. Based on the Irwin analytical model accordance with equation 14, CPZS in-plane strain condition is correlated with load range (ΔK). In the Irwin analytic relationship, elastic- perfectly plastic behavior was applied with von-Mises yield criterion. This material model is a simplistic assumption that decreases the accuracy of the prediction of the plastic zone, while the Chaboche advanced model presents the hardening behavior of the material in cyclic loading, which is consistent with experimental results. This model, which has been tested on the studied material, was implemented in the finite element software. For comparison, in Fig. 14, the

stress-strain behavior of the studied material is presented in elastic-perfectly plastic model and Chaboche nonlinear kinematic hardening model in the cyclic loading branch (Fig. 4). As shown in Fig. 14, the presence of kinematic hardening in the stable loop increases the yield level after the cyclic yield point. Figs. 15a, 15b, and 15c show the CPZS based on the finite element model and the analytic model of equation (15).

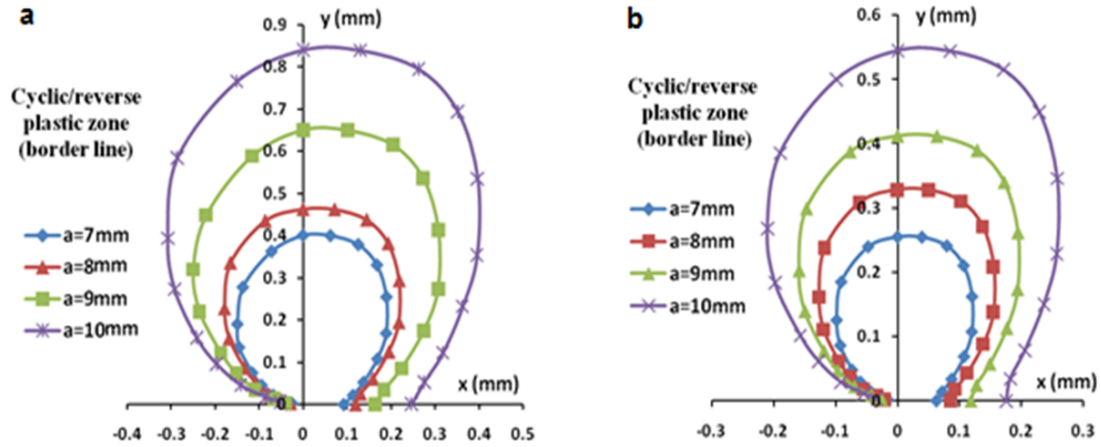

Fig. 9. Plastic zone versus crack lengths for $P_{max} = 1200$N, a) $R = 0.1$, b) $R = 0.3$.

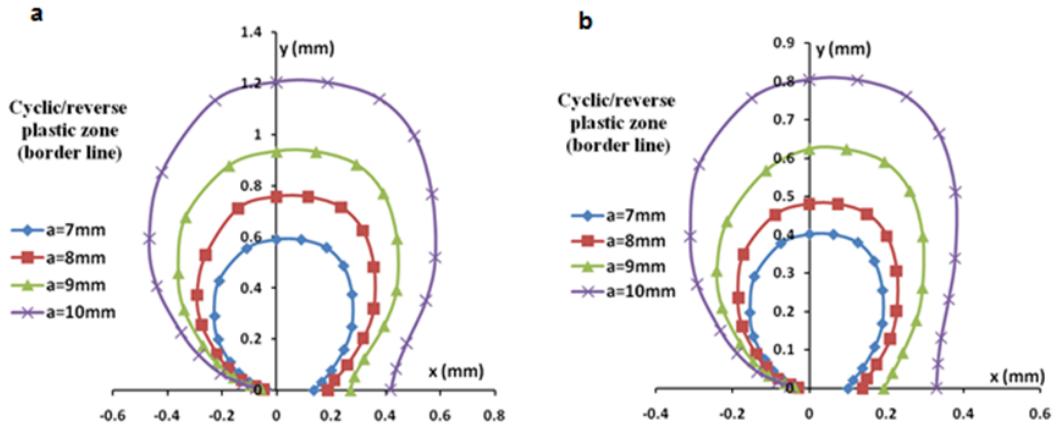

Fig. 10. Cyclic plastic zone versus crack lengths for $P_{max} = 1200$N, a) $R = 0.1$, b) $R = 0.3$.

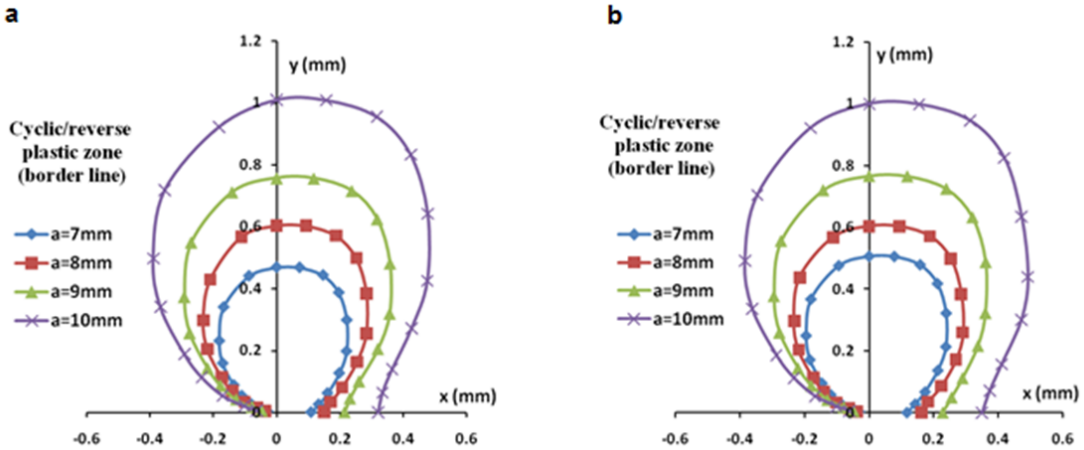

Fig. 11. Cyclic plastic zone versus crack lengths for $\Delta P = 1200$N, a) $E = 0.077$, b) $R = 0.2$.

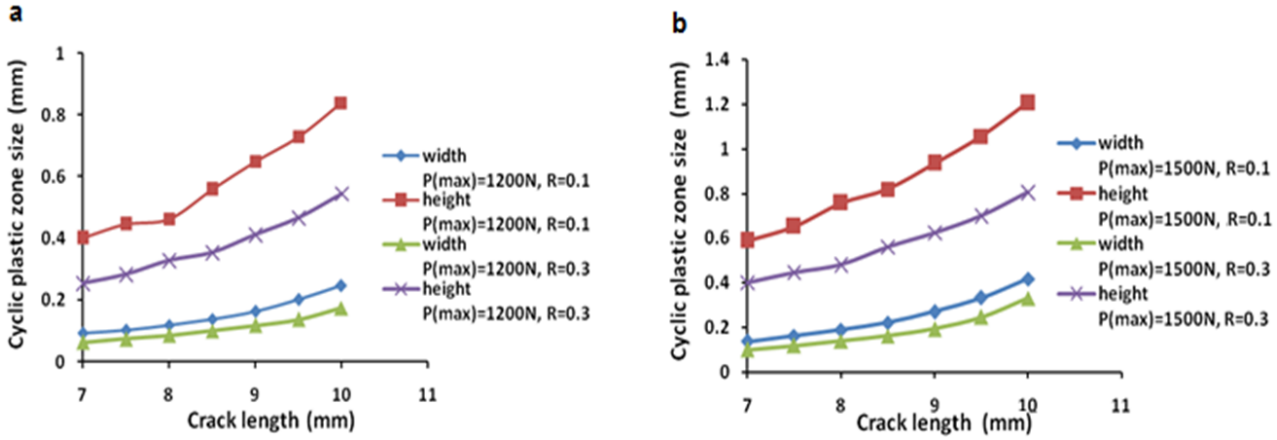

Fig. 12. Width and height of the CPZs for different crack lengths and $R = 0.1, 0.3$ a) $\Delta P = 1.2$kN, b) $\Delta P = 1.5$kN.

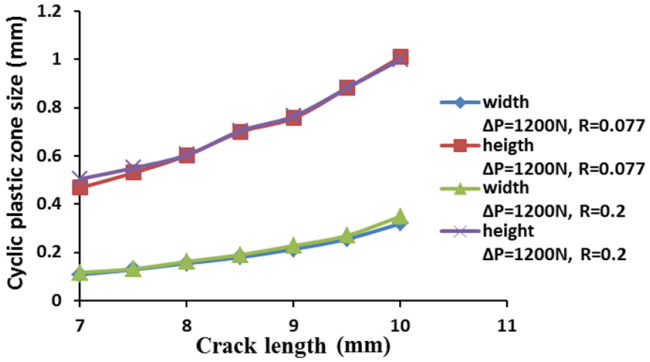

Fig. 13. Width and height of the CPZs at fixed load range $\Delta = 1.2$kN and different load ratios $R = 0.077$, $R = 0.2$ for different crack lengths;

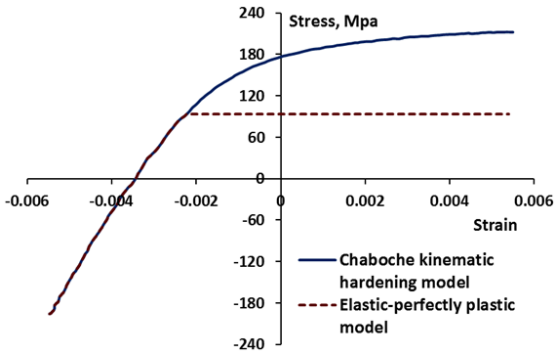

Fig. 14. The loading branches of stress-strain curves based on the Chaboche nonlinear kinematic hardening and elastic-perfectly plastic models for pure copper.

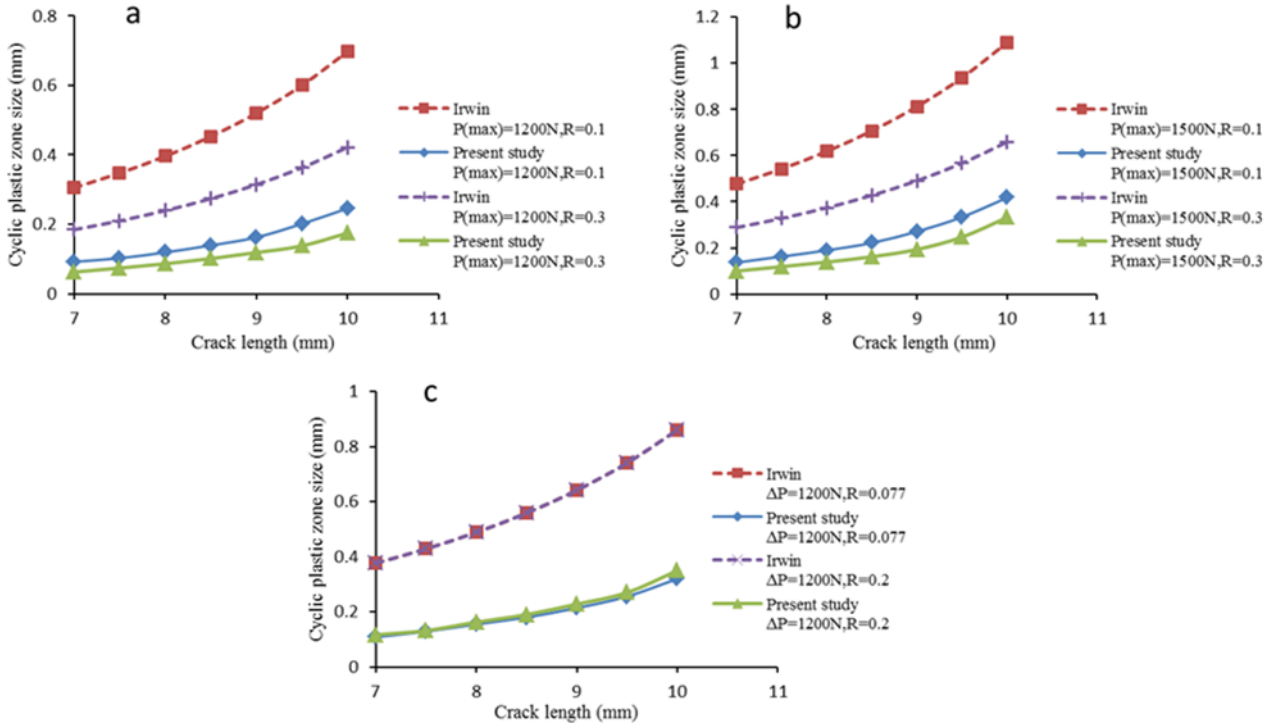

Fig. 15. Analytic and finite element models prediction of CPSZ, a) $P_{max} = 1.2$kN, b) $P_{max} = 1.5$kN, c) $\Delta P = 1.2$kN.

As shown in Figs. 15a and 15b, in total loadings, the CPZS obtained from the analytic model is larger than that of finite element model. The values of CPZS in two models have large differences because the analytic model does not consider the hardening behavior of the studied material in cyclic loading. This limitation leads to unreliability of the predictions of this model. Numerical analyses show that increasing the crack length under the same loading conditions leads to an increase in the size of the plastic zone around the crack tip. This is also due to the analytical model because the increase in the length of the crack leads to an increase in the range of stress intensity factor according to Eq. 12 and thus CPZS increases according to Eq. 14. In fact, the enlargement of the plastic zone with crack growth decreases the material strength against crack growth. In a model with the hardening behavior compared to an analytical model that considers material behavior as an elastic-perfectly plastic, the increase in the yield level of material after the cyclic yield point (Fig. 14) leads to a decrease in CPZS.

6. Conclusions

In this study, the effects of the nonlinear kinematic hardening on the shapes and CPZSs were investigated using finite element simulation. Analytical and numerical solutions based on the monotonic loading behavior can lead to a significant error. Moreover analytical models, such as the Irwin and Dugdale models, consider the material behavior as elastic-perfectly plastic, whilst many materials such as pure copper, have elastic-plastic behavior and exhibit high kinematic hardening behavior under the cyclic loadings. The Chaboche model is selected for use in the finite element analysis, due to its precision in the modeling of the nonlinear kinematic hardening behavior. The parameters of the hardening model were extracted from experimental tests with symmetric strain-controlled cyclic loading. When the hysteresis loops were formed in the cyclic loading, the cyclic plastic zone was created. Numerical solutions in present study were performed in different crack lengths under different loading conditions. The simulation results showed that the CPZS, unlike the monotonic plastic zone, does not depend on the maximum load and depends only on the load range. The results in this study showed that the CPZS increases by fixing the maximum load, P_{max} and decreasing the load ratio. The results of the Irwin analytical model were compared with the simulation results, which uses the Chaboche kinematic hardening model in the finite element analysis. The results showed that the CPZS in the finite element model was significantly different from the Irwin model results and had fewer values. The small size of this plastic zone is because of its nonlinear kinematic hardening behavior. According to the results of this study, CPZS increases with increasing the cracks length. Considering that increase in the crack length in fatigue loading leads to increasing the crack growth rate, the cyclic plastic zone could be an appropriate criterion for fatigue crack growth analysis. In fact, the cyclic plastic zone is of great importance, because it absorbs a high percentage of energy of the system and can be a significant parameter in the analysis of the fatigue crack growth, such as δK, cyclic J-integral, and crack tip opening displacement.

References

[1] P. Paris, F. Erdogan, A critical analysis of crack propagation laws. J. Basic. Eng., 85(4) (1963) 528-533.

[2] S.K. Paul, Numerical models of plastic zones and associated deformations for a stationary crack in a C (T) specimen loaded at different R-ratios, Theo, Appl. Frac. Mech., 84 (2016) 183-191.

[3] S. Mishra, B. Parida, A study of crack-tip plastic zone by elastoplastic finite element analysis. Eng. Frac. Mech., 22(6) (1985) 951-956.

[4] Y. Iino, Fatigue crack propagation work coefficienta material constant giving degree of resistance to fatigue crack growth, Eng. Frac. Mech., 12(2) (1979) 279-299.

[5] R. McClung, Crack closure and plastic zone sizes in fatigue, Fatig. Frac. Eng. Mat. Struct., 14(4) (1991) 455-468.

[6] G.R. Irwin, Plastic zone near a crack and fracture toughness, Proceedings, 7th sagamore conference, IV (1960) 63-78.

[7] D.S. Dugdale, Yielding of steel sheets containing slits, J. Mech. Phys. Sol., 8(2) (1960) 100-104.

[8] C. Jingjie, H. Yi, D. Leilei, L. Yugang, A new method for cyclic crack-tip plastic zone size determination under cyclic tensile load, Eng. Frac. Mech., 126 (2014) 141-154.

[9] B.O. Chikh, A. Imad, M. Benguediab, Influence of the cyclic plastic zone size on the propagation of the fatigue crack in case of 12NC6 steel, Comput. Mat. Sc., 43(4) (2008) 1010-1017.

[10] S. Kwun, M. Fine, Dependence of cyclic plastic work of fatigue crack propagation on K in MA87 A1 P/M alloy, Scripta Metallurgica, 14(1) (1980) 155-158.

[11] J. Rice, Mechanics of crack tip deformation and extension by fatigue, in Fatigue crack propagation, ASTM International, (1967).

[12] R.H. Hertzberg, R.P. Vinci,J.L. Hertzberg, Deformation and fracture mechanics of engineering materials, 5 ed. John Wiley and Sons, (2012).

[13] R. Seifi, R. Bahrami, Numerical modeling the effects of overloading and underloading in fatigue crack growth, Eng. Fail. Anal., 17(6) (2010) 1475-1482.

[14] Y. Jiang, J. Zhang, Benchmark experiments and characteristic cyclic plasticity deformation. Int. J. Plast., 24(9) (2008) 1481-1515.

[15] S.K. Paul, S. Sivaprasad, S. Dhar, M. Tarafder, S. Tarafder, Simulation of cyclic plastic deformation response in SA333 CMn steel by a kinematic hardening mode, Comput. Mat. Sci., 48(3) (2010) 662-671.

[16] S.K. Paul, S. Tarafder, Cyclic plastic deformation response at fatigue crack tips, Int. J. Press. Ves. Pip., 101 (2013) 81-90.

[17] J.L. Chaboche, Time-independent constitutive theories for cyclic plasticity, Int. J. Plast., 2(2) (1986) 149-188.

[18] C.O. Frederick, P. Armstrong, A mathematical representation of the multiaxial Bauschinger effect. Mater. High. Temp., 24(1) (2007) 1-26.

[19] N. Ohno, J.D. Wang, Kinematic hardening rules with critical state of dynamic recovery, part I: formulation and basic features for ratchetting behavior, Int. J. Plast., 9(3) (1993) 375-390.

[20] W. Prager, Recent developments in the mathematical theory of plasticity, J. Appl. Physic., 20(3) (1949) 235-241.

[21] S. Bari, T. Hassan, Anatomy of coupled constitutive models for ratcheting simulation, Int. J. Plast., 16(3-4) (2000) 381-409.

[22] E606/E606M-12, Standard Test Method for Strain-Controlled Fatigue Testing, ASTM International, West Conshohocken (PA USA): Book of Standards, (2012).

[23] E. Gdoutos, Solid mechanics and its applications-fracture mechanics, Springer, The Netherlands, (2005).

[24] ASTM, E647-08, Standard test method for measurement of fatigue crack growth rates, ASTM International: West Conshohocken, PA, (2008).